nature geoscience

LETTERS

PUBLISHED ONLINE: 2 MAY 2016 | DOI: 10.1038/NGEO2705

# Airborne soil organic particles generated by precipitation

Bingbing Wang[1†], Tristan H. Harder[2,3], Stephen T. Kelly[2†], Dominique S. Piens[2], Swarup China[1], Libor Kovarik[1], Marco Keiluweit[4], Bruce W. Arey[1], Mary K. Gilles[2] and Alexander Laskin[1*]

**Airborne organic particles play a critical role in Earth's climate[1], public health[2], air quality[3], and hydrological and carbon cycles[4]. However, sources and formation mechanisms for semi-solid and solid organic particles[5] are poorly understood and typically neglected in atmospheric models[6]. Laboratory evidence suggests that fine particles can be formed from impaction of mineral surfaces by droplets[7]. Here, we use chemical imaging of particles collected following rain events in the Southern Great Plains, Oklahoma, USA and after experimental irrigation to show that raindrop impaction of soils generates solid organic particles. We find that after rain events, sub-micrometre solid particles, with a chemical composition consistent with soil organic matter, contributed up to 60% of atmospheric particles. Our irrigation experiments indicate that intensive water impaction is sufficient to cause ejection of airborne soil organic particles from the soil surface. Chemical imaging and micro-spectroscopy analysis of particle physico-chemical properties suggest that these particles may have important impacts on cloud formation and efficiently absorb solar radiation. We suggest that raindrop-induced formation of solid organic particles from soils may be a widespread phenomenon in ecosystems such as agricultural systems and grasslands where soils are exposed to strong, episodic precipitation events[8].**

For the first time, a large population of highly viscous (glassy) carbonaceous particles was observed in a sample collected at the Southern Great Plains site in Lamont, Oklahoma, USA. The striking feature was the abundant appearance of solid particles that did not deform on impaction (Fig. 1). These spherical particles appear as bright features (Fig. 2a) with high vertical dimensions (height-to-base aspect ratios) in scanning electron microscopy (SEM) images (Fig. 2b). In the sample collected on 27 March 2014, analysis of SEM images indicated that nearly 60% of all particles were solid organic particles with characteristic aspect ratios of 0.8–1.0 (Supplementary Fig. 1). X-ray microanalysis indicates they are comprised primarily of C, O and N (Fig. 2c). The appearance of these solid organic particles was unexpected; hence, further samples were collected on 23 September and 2 October 2014 (Fig. 2d,e). Although the presence of solid organic particles was significant (~30%) in both of the subsequent samples, their relative abundance was less than in the sample collected on 27 March 2014. In all samples, the solid organic particles have a fairly narrow size distribution centred at ~0.6 μm (Fig. 2f). According to the backward air trajectories, air masses arriving at the Southern Great Plains site during these sampling dates originated from very different directions and lacked any common trend (Supplementary Fig. 2). Although, initially, the nature of these unusual solid organic particles was puzzling, their reoccurrence in multiple samples, with dissimilar back trajectories, indicated a persistent local source rather than regional transport.

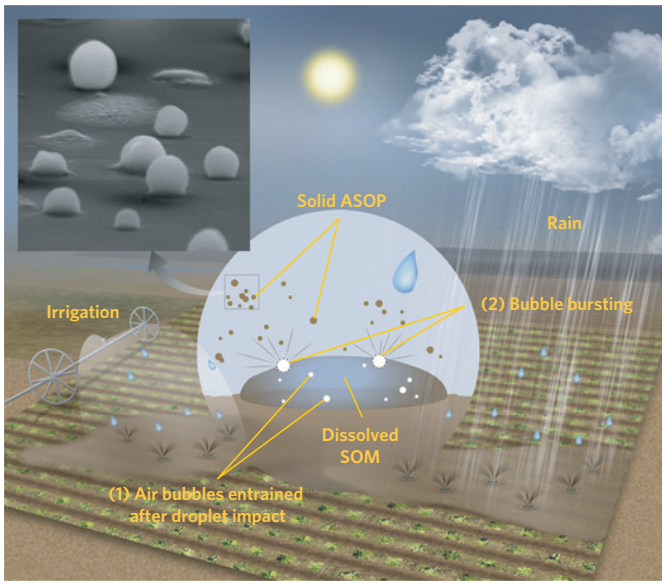


**Figure 1 | A schematic illustration of the 'raindrop' mechanism[7] generating airborne soil organic particles (ASOP).** (1) Raindrops impinging on the soil surface entrain air bubbles into the surface water layer containing dissolved soil organic matter (SOM). (2) The bubbles burst at the air/water interface and eject ASOP that solidify to become glassy particles on drying. The insert in the upper left corner shows a scanning electron micrograph image of glassy ASOP collected at the Southern Great Plains site.

Chemical imaging of the solid particles using X-ray absorption micro-spectroscopy (Figs 3 and 4) indicated their chemical composition resembled typical soil organic matter (SOM; Fig. 4a). This similarity prompted the hypothesis that we observed airborne soil organic particles (ASOP) generated by a 'raindrop' mechanism suggested by Joung and Buie[7], who monitored a fine aqueous mist ejected from droplets impinging onto mineral surfaces in laboratory

[1]William R. Wiley Environmental Molecular Sciences Laboratory, Pacific Northwest National Laboratory, Richland, Washington 99354, USA. [2]Chemical Sciences Division, Lawrence Berkeley National Laboratory, Berkeley, California 94720, USA. [3]Department of Chemistry, University of California, Berkeley, California 94720, USA. [4]Stockbridge School of Agriculture, University of Massachusetts, Amherst, Massachusetts 01003, USA. [†]Present addresses: State Key Laboratory of Marine Environmental Science and College of Ocean and Earth Sciences, Xiamen University, Xiamen 361102, China (B.W.); Carl Zeiss X-ray Microscopy Inc., Pleasanton, California 94588, USA (S.T.K.). *e-mail: Alexander.Laskin@pnnl.gov

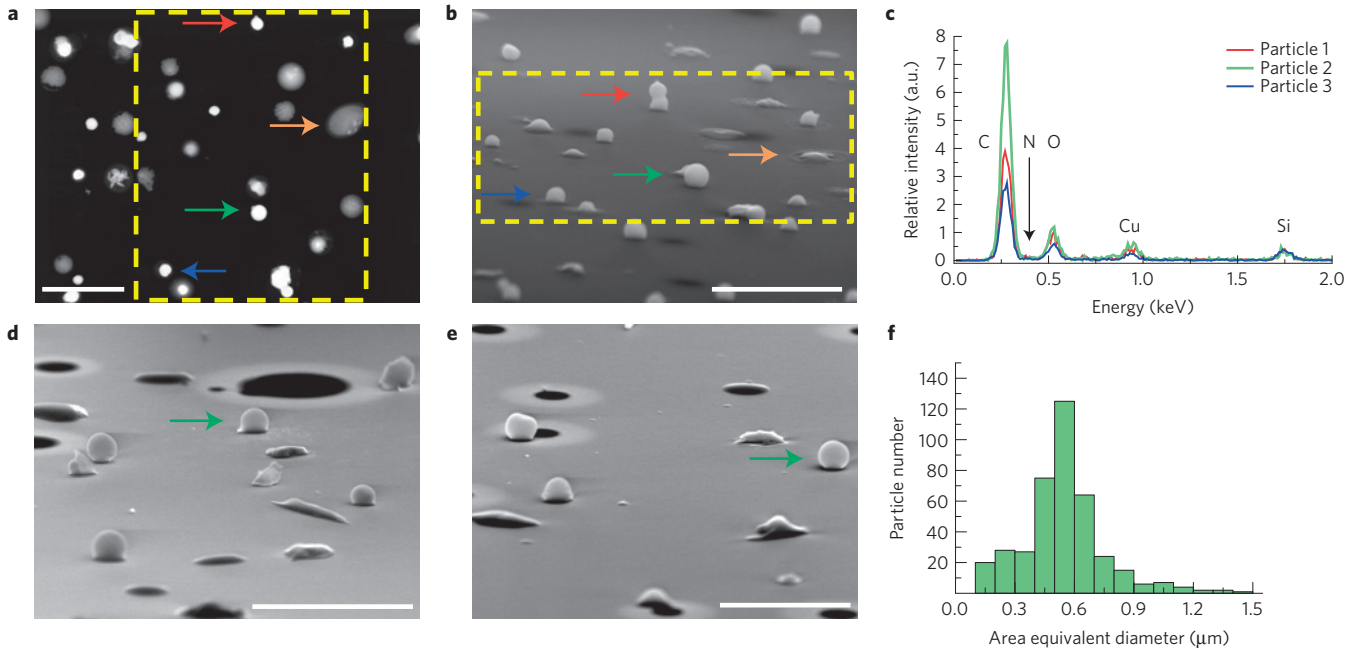


**Figure 2 | Morphology, size distribution and elemental composition of ASOP. a**, Scanning electron microscopy (SEM) image (in the forward-scattered transmitted electron mode) of particles collected at the Southern Great Plains site (27 March 2014). **b**, SEM image (in the secondary electron mode) of the same sample at 75° tilt angle. The yellow boxes indicate the identical area. **c**, Energy dispersive X-ray spectra of ASOP marked by the red, green and blue arrows in **a** and **b**. Orange arrow indicates a sulfur-containing particle. **d**,**e**, Tilt angle SEM images of particles collected at the site on 23 September and 2 October 2014, respectively. **f**, Size distribution of the ASOP. Scale bars are 4 μm.

experiments. The droplets induced intense generation of bubbles within a layer of the impinged droplets, followed by ejection of fine particles on bursting of the bubbles at the air–water interface, analogous to the well-known bubble-bursting process of sea spray generation[9]. Joung and Buie suggested that rainfall may generate fine sub-micrometre aerosol from soils[7]. Indeed, analysis of the rain rates and particle concentration records from the Southern Great Plains site indicate a very strong rain event occurred the day before sampling on 27 March and coincident with the increased concentration of ~0.6 μm particles (Supplementary Fig. 3). Shorter rain events also preceded sampling on 23 September and 2 October (Supplementary Table 1). However, there is no obvious correlation between the fraction of ASOP and amount of rainfall or intensity of rainfall. To test the 'raindrop' hypothesis of ASOP generation, a proof-of-concept experiment was performed. A section of garden topsoil was sprinkled with a garden hose until it was well irrigated. This was followed by sampling of airborne particles above the soil surface. ASOP with characteristic near-spherical (glassy) shapes were unambiguously detected in this sample, consistent with an origin from the 'raindrop' mechanism (Supplementary Fig. 4).

Assessment of the particle phase, carbon bonding, oxygen-to-carbon ratio, and total carbon absorption characteristic of ASOP was performed based on X-ray micro-spectroscopy data (Figs 3 and 4 and Supplementary Fig. 5). Similarly sized carbonaceous particles with higher total carbon absorption are more viscous or solid (glassy) than those with lower absorption, which is indicative of liquid particles flattened on the substrate[10]. Figure 3c illustrates the heights of the ASOP as a function of particle size (determined as the two-dimensional (2D) projected area equivalent diameter), compared with other organic particles observed at the Southern Great Plains site and previously reported measurements[10]. For a given particle size, ASOP have total carbon absorption values up to ten times larger than particles observed in previous studies[10]. This indicates that ASOP are significantly more viscous (solid) than organic particles reported previously. Further, they may represent a distinctly different particle type with a unique production mechanism.

The carbon near-edge X-ray absorption fine structure (NEXAFS) spectra of ASOP are remarkably different from those typical for atmospheric soot or biogenic secondary organic aerosols (Fig. 4a). Unlike the spatially resolved NEXAFS of typical mixed soot/organic particles, where the most intense C=C carbon is in isolated inclusions[11], in the ASOP the enhanced carbon–carbon double bonds are homogeneously distributed throughout the particles (Fig. 4b). An elemental ratio of $C_{23}N_{x<3}O_{10}$ was derived for ASOP based on carbon, oxygen and nitrogen K-edge NEXAFS spectra acquired over the identical particles (Supplementary Fig. 5). The NEXAFS spectra of ASOP have some resemblance to the tar balls' spectra. However, the normalized carbon–carbon double bond peak area (C=C, $sp^2$ hybridization) of ASOP is three times larger than that observed for tar balls. Furthermore, the characteristic size distribution modes of tar balls from biomass smoke samples are centred at 100–300 nm (refs 12–14), or approximately half the mode size (600 nm) of ASOP. Also, no other characteristic biomass burning particles such as soot or potassium salts were detected in these samples. Hence, the ASOP are neither tar balls nor internal mixtures of soot and organics, but rather a separate, distinct type of atmospheric particles. The total carbon absorption/area equivalent diameter ratio is indicative of ASOP solidity, and is positively correlated with $sp^2$ (C=C) hybridization (Fig. 4c). The majority of ASOP have values of total carbon absorption/area equivalent diameter ratio $>0.5\,\mu m^{-1}$ and $sp^2$ hybridization >20%, respectively.

The qualitative similarity (Fig. 4a) between NEXAFS spectra of ASOP, tar balls, and 'free light' SOM isolated in a study (Methods, X-ray spectroscopy of soil samples) from the surface layers of agricultural soils is notable, and suggests a plausible interrelation of their composition. Indeed, composition of the tar balls is attributed to the organic materials ejected from the pores of burning plants, emitted first as fine liquid particles, and later solidified by heat[15].

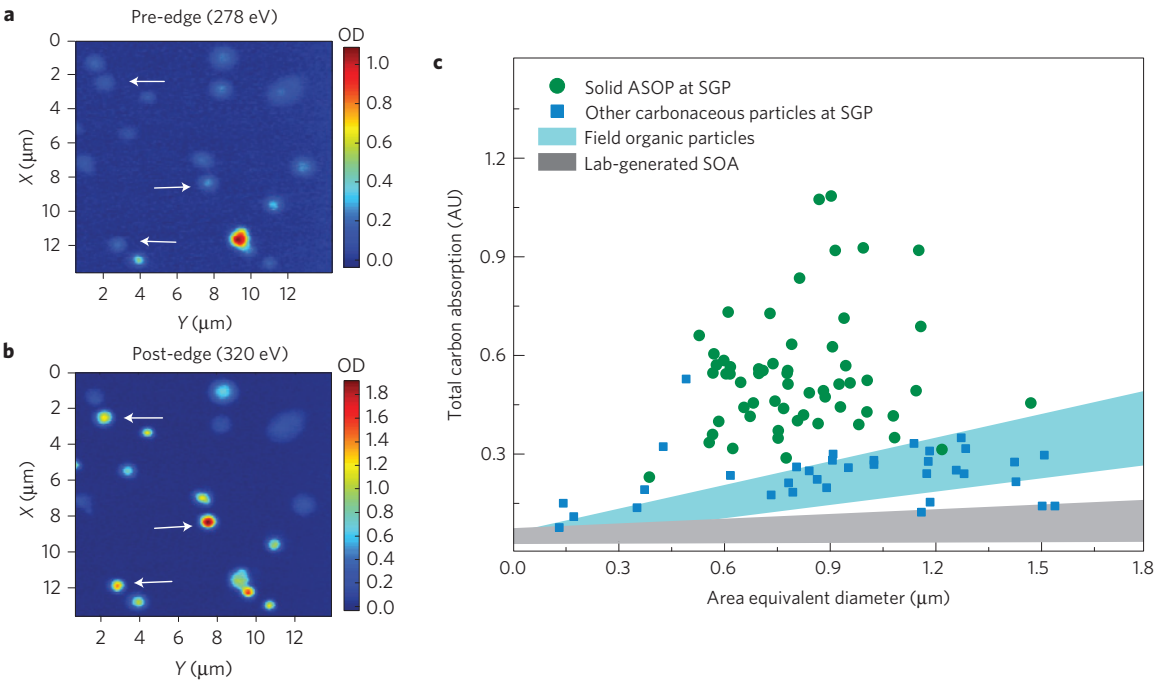


**Figure 3 | Optical density (OD) and phase state of the ASOP obtained from X-ray micro-spectroscopy. a**,**b**, Pre-edge (**a**) and post-edge (**b**) OD maps of particles collected at the Southern Great Plains (SGP) site (the same field of view is shown in two maps). ASOP are indicated by the arrows. **c**, Plot of total carbon absorption (TCA) as a function of area equivalent diameter (AED) for individual carbonaceous particles detected in present and previous[10] studies. High absorptions at the pre-edge and post-edge indicate the inorganic and total carbon content, respectively. The plots indicate stronger absorption of X-rays by solid ASOP than any other similarly sized organic particles. AU, absorbance units; SOA, secondary organic aerosol.

Plant-derived products, such as polysaccharides, tannins, and lignin fragments, are also major components of 'free light' SOM (ref. 16). These components are only loosely associated with the soil matrix; thus, soluble components may be prone to aerosolization through a 'raindrop' mechanism. The molecular constituents of SOM are substantially larger than common atmospheric organics[17]. Assuming $>C_{18}$ molecules (MW $>$ 250 g mol$^{-1}$) are dominant in mobilized SOM (ref. 18) and the O/C ratio of ~0.4 reported here, based on the compilations of Koop *et al.*[5] we estimate a glass transition temperature of SOM of ~300 K. Therefore, evaporation of water from the SOM-containing mist would result in amorphous solidification (glassy state) at ambient temperatures, consistent with observations of solid spherical ASOP reported here (Supplementary Fig. 6). Furthermore, ASOP appear as uncoated or have visible coatings on their surfaces (Supplementary Fig. 7). This indicates that ASOP are generated as primary particles and their surfaces promote heterogeneous chemistry and condensation of secondary species. Although similarities between NEXAFS fingerprints of SOM and ASOP (Fig. 4a) allow us to infer the source and mechanism of ASOP formation, depending on the variability of the soils at different geographical locations, ASOP composition may vary. For instance, ASOP sampled in the irrigation experiment have substantially more oxygen-containing functionalities than those collected at the SGP site, as indicated by characteristic peaks in their NEXAFS spectra (Supplementary Fig. 4).

At present, it is assumed that particles from soils enter the atmosphere primarily through wind erosion or human activities such as agricultural tilling or harvesting. The observations of solid ASOP reported here challenge our understanding of the sources and formation mechanisms of atmospheric organic particles, and suggest an additional source from atmosphere—land surface interactions. The SOM-derived composition of ASOP implies their inherent relevance to atmospheric brown carbon and their plausible contribution to the absorption and scattering of solar and terrestrial radiation[19]. Estimates of ASOP optical properties based on reported correlations[20] with the O/C ratio and the $sp^2$ hybridization suggest values of single scattering albedo of 0.8–1.0 and Ångström absorption coefficients of 1.5–3.5—characteristic of brown carbon, respectively. Dynamic environmental SEM imaging of hydrating ASOP (Supplementary Fig. 8) shows that ASOP would serve as cloud condensation nuclei at atmospherically relevant supersaturations, and potentially impact the formation of warm clouds. At higher altitudes, ASOP would provide solid glass surfaces for heterogeneous ice nucleation in cirrus and mixed-phase clouds. Notably, the importance of SOM as strong ice nuclei has been explicitly reported in field and laboratory studies dating back to the early seventies[21]. More recently, it has been explicitly shown that particles containing SOM proxy material can be in the solid phase and serve as efficient ice nuclei[22]. However, airborne SOM has always been attributed to soil erosion; SOM emitted by means of a rainfall mechanism have not been considered. In addition, emissions of ASOP may be influenced by a feedback loop of the regional rainfall enhancement due to the expanding developments in cropland irrigation[23].

Initially, it was fairly surprising that ASOP have not been previously reported. However, there are compelling reasons for the lack of ASOP observations. ASOP are refractory and do not decompose substantially on heating up to 600 °C (Supplementary Fig. 9), implying that they would not be detected by evaporation-based methods of *in-situ* particle analysis. Thus, if ASOP were present, the organic particle concentration measured by evaporation-based methods would be underestimated. Laser ablation mass spectrometry could detect ASOP; however, extensive fragmentation of the organic material on ablation would render interpretation of the spectra challenging, and they could be confused with other organic particles. Because of their solid phase and SOM-based composition, microscopy and microanalysis methods may be the most effective tools for detection of ASOP. However,

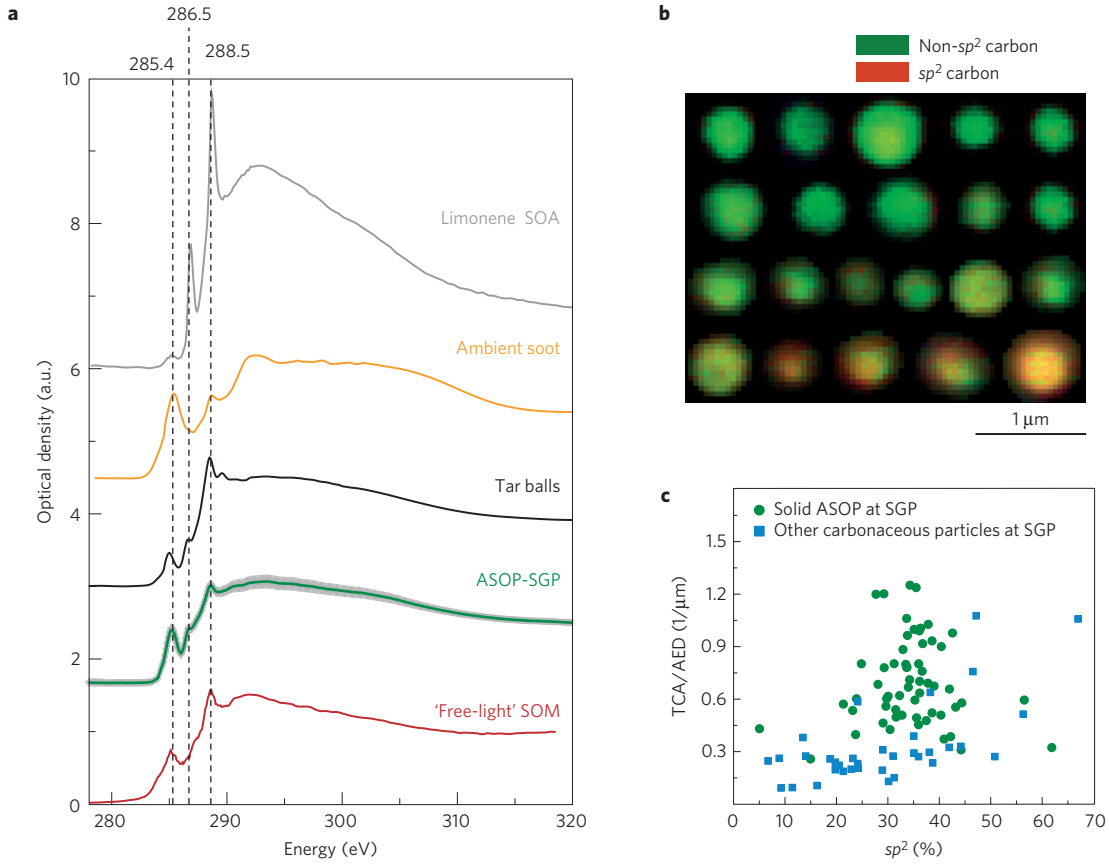


**Figure 4 | Carbon chemical bonding and mixing state of the ASOP obtained from X-ray micro-spectroscopy. a**, Carbon K-edge spectra of ASOP (37 particles averaged, variability is shown by the grey shaded region) compared to: tar balls (150 particles averaged), ambient soot, and limonene secondary organic aerosol (SOA). Dashed lines indicate the absorption by C=C bonding ($sp^2$, 285.4 eV), the -COOH (288.5 eV) and R(C=O)R/C-OH (286.5 eV) functional groups. **b**, ASOP compositional maps with $sp^2$ (C=C) and non-$sp^2$ carbon shown in red and green, respectively. **c**, Correlation between the total carbon absorption/area equivalent diameter (TCA/AED) ratio and $sp^2$ carbon content for carbonaceous particles detected in the Southern Great Plains (SGP) samples.

initial distinction of solid ASOP from other particles occurred when images were acquired over tilted samples (Fig. 2). Previously, acquisition of tilt angle SEM images of atmospheric aerosol particles has not been a common practice. Furthermore, most microscopy studies of particle chemistry have focused on samples collected in polluted areas, whereas sampling at rural areas and surrounding rain events (where ASOP are expected) were less common.

Although there are no explicit reports of ASOP, the assumption of their widespread existence in the atmosphere is consistent with some published observations. For example, a month of measurements at the Southern Great Plains site during May 2003 noted the frequent appearance of weakly hygroscopic 430–600 nm particles (ratio of wet-to-dry diameters $D/D^* = 1.1$ at RH 85%)[24]. Because of their low hygroscopicity, those particles were attributed to mineral dust. However, on the basis of the ASOP characteristics presented here (Fig. 2 and Supplementary Fig. 8), it is reasonable to suggest that those particles were perhaps ASOP. Also, numerous studies have reported enhancement of fluorescent particles after rain events[25–28]. Large super-micrometre fluorescent particles are commonly attributed to biogenic spores, bacteria, fungi, and so on. However, because of their SOM nature, ASOP would also have a strong fluorescence signal[29] and some of these sub-micrometre fluorescent particles[27,28] may have been ASOP. Furthermore, elevated concentrations of ice nucleating particles detected[27,28] after rainfall might be also partially related to ASOP. Finally, a slightly counterintuitive observation[30] that stronger and more widespread rain, in a tropical rural location in India, resulted in a smaller reduction and faster recovery of the aerosol optical depth than less intense rainfall, may again be in line with the ASOP formation.

Future studies should further explore the atmosphere—land surface interactions by assessing the relationship between rainfall intensity and efficiency of ASOP generation, evaluate and constrain ASOP budgets at different geographic areas, describe area-specific variability in the ASOP composition, and quantify the optical and cloud nucleation properties of ASOP.

## Methods

Methods and any associated references are available in the online version of the paper.

Received 1 November 2015; accepted 29 March 2016; published online 2 May 2016

## References

1. Boucher, O. *et al*. in *Climate Change 2013: The Physical Science Basis* (eds Stocker, T. F. *et al*.) 571–658 (IPCC, Cambridge Univ. Press, 2013).
2. Poeschl, U. & Shiraiwa, M. Multiphase chemistry at the atmosphere-biosphere interface influencing climate and public health in the anthropocene. *Chem. Rev.* **115,** 4440–4475 (2015).
3. von Schneidemesser, E. *et al*. Chemistry and the linkages between air quality and climate change. *Chem. Rev.* **115,** 3856–3897 (2015).
4. Hopkins, F. M., Torn, M. S. & Trumbore, S. E. Warming accelerates decomposition of decades-old carbon in forest soils. *Proc. Natl Acad. Sci. USA* **109,** E1753–E1761 (2012).

5. Koop, T., Bookhold, J., Shiraiwa, M. & Poschl, U. Glass transition and phase state of organic compounds: dependency on molecular properties and implications for secondary organic aerosols in the atmosphere. *Phys. Chem. Chem. Phys.* **13,** 19238–19255 (2011).
6. Bones, D. L., Reid, J. P., Lienhard, D. M. & Krieger, U. K. Comparing the mechanism of water condensation and evaporation in glassy aerosol. *Proc. Natl Acad. Sci. USA* **109,** 11613–11618 (2012).
7. Joung, Y. S. & Buie, C. R. Aerosol generation by raindrop impact on soil. *Nature Commun.* **6,** 6083 (2015).
8. Cotrufo, M. F. *et al*. Formation of soil organic matter via biochemical and physical pathways of litter mass loss. *Nature Geosci.* **8,** 776–779 (2015).
9. Blanchard, D. C. & Woodcock, A. H. Bubble formation and modification in the sea and its meteorological significance. *Tellus* **9,** 145–158 (1957).
10. O' Brien, R. E. *et al*. Physical properties of ambient and laboratory-generated secondary organic aerosol. *Geophys. Res. Lett.* **41,** 4347–4353 (2014).
11. Moffet, R. C. *et al*. Spectro-microscopic measurements of carbonaceous aerosol aging in Central California. *Atmos. Chem. Phys.* **13,** 10445–10459 (2013).
12. Tivanski, A. V., Hopkins, R. J., Tyliszczak, T. & Gilles, M. K. Oxygenated interface on biomass burn tar balls determined by single particle scanning transmission X-ray microscopy. *J. Phys. Chem. A* **111,** 5448–5458 (2007).
13. Posfai, M. *et al*. Atmospheric tar balls: particles from biomass and biofuel burning. *J. Geophys. Res. Atmos.* **109,** D06213 (2004).
14. Chakrabarty, R. K. *et al*. Brown carbon in tar balls from smoldering biomass combustion. *Atmos. Chem. Phys.* **10,** 6363–6370 (2010).
15. Toth, A., Hoffer, A., Nyiro-Kosa, I., Posfai, M. & Gelencser, A. Atmospheric tar balls: aged primary droplets from biomass burning? *Atmos. Chem. Phys.* **14,** 6669–6675 (2014).
16. Marin-Spiotta, E., Swanston, C. W., Torn, M. S., Silver, W. L. & Burton, S. D. Chemical and mineral control of soil carbon turnover in abandoned tropical pastures. *Geoderma* **143,** 49–62 (2008).
17. Graber, E. R. & Rudich, Y. Atmospheric HULIS: How humic-like are they? A comprehensive and critical review. *Atmos. Chem. Phys.* **6,** 729–753 (2006).
18. Spaccini, R., Baiano, S., Gigliotti, G. & Piccolo, A. Molecular characterization of a compost and its water-soluble fractions. *J. Agric. Food Chem.* **56,** 1017–1024 (2008).
19. Laskin, A., Laskin, J. & Nizkorodov, S. A. Chemistry of atmospheric brown carbon. *Chem. Rev.* **115,** 4335–4382 (2015).
20. Hopkins, R. J. *et al*. Correlations between optical, chemical and physical properties of biomass burn aerosols. *Geophys. Res. Lett.* **34,** L18806 (2007).
21. Schnell, R. C. & Vali, G. Atmospheric ice nuclei from decomposing vegetation. *Nature* **236,** 163–165 (1972).
22. Wang, B. & Knopf, D. A. Heterogeneous ice nucleation on particles composed of humic-like substances impacted by $O_3$. *J. Geophys. Res. Atmos.* **116,** D03205 (2011).
23. Alter, R. E., Im, E.-S. & Eltahir, E. A. B. Rainfall consistently enhanced around the Gezira Scheme in East Africa due to irrigation. *Nature Geosci.* **8,** 763–767 (2015).
24. Gasparini, R., Li, R. J., Collins, D. R., Ferrare, R. A. & Brackett, V. G. Application of aerosol hygroscopicity measured at the atmospheric radiation measurement program's southern great plains site to examine composition and evolution. *J. Geophys. Res. Atmos.* **111,** D05S12 (2006).
25. Bigg, E. K., Soubeyrand, S. & Morris, C. E. Persistent after-effects of heavy rain on concentrations of ice nuclei and rainfall suggest a biological cause. *Atmos. Chem. Phys.* **15,** 2313–2326 (2015).
26. Huffman, J. A. *et al*. High concentrations of biological aerosol particles and ice nuclei during and after rain. *Atmos. Chem. Phys.* **13,** 6151–6164 (2013).
27. Prenni, A. J. *et al*. The impact of rain on ice nuclei populations at a forested site in Colorado. *Geophys. Res. Lett.* **40,** 227–231 (2013).
28. Schumacher, C. J. *et al*. Seasonal cycles of fluorescent biological aerosol particles in boreal and semi-arid forests of Finland and Colorado. *Atmos. Chem. Phys.* **13,** 11987–12001 (2013).
29. Zsolnay, A., Baigar, E., Jimenez, M., Steinweg, B. & Saccomandi, F. Differentiating with fluorescence spectroscopy the sources of dissolved organic matter in soils subjected to drying. *Chemosphere* **38,** 45–50 (1999).
30. Saha, A. & Moorthy, K. K. Impact of precipitation on aerosol spectral optical depth and retrieved size distributions: a case study. *J. Appl. Meteorol.* **43,** 902–914 (2004).


## Acknowledgements

We are grateful to K. Teske and P. Dowell for assistance in sample collection at the Southern Great Plains site. The Pacific Northwest National Laboratory (PNNL) group acknowledges support from the Chemical Imaging Initiative of the Laboratory Directed Research and Development Program at PNNL. The Lawrence Berkeley National Laboratory (LBNL) group acknowledges support from the US Department of Energy's Atmospheric System Research Program, an Office of Science, Office of Biological and Environmental Research (OBER). The CCSEM/EDX, TEM and helium ion microscopy analyses were performed at Environmental Molecular Sciences Laboratory, a National Scientific User Facility sponsored by OBER at PNNL. PNNL is operated by the US Department of Energy by Battelle Memorial Institute under contract DE-AC06-76RL0. STXM/NEXAFS analysis at beamlines 5.3.2 and 11.0.2 of the Advanced Light Source at LBNL is supported by the Director, Office of Science, Office of Basic Energy Sciences of the US Department of Energy under Contract No. DE-AC02- 05CH11231. Beamline 11.0.2 also acknowledges support from the Office of Basic Energy Sciences Division of Chemical Sciences, Geosciences, and Biosciences by the Condensed Phase and Interfacial Molecular Sciences Program of the US Department of Energy. Soil NEXAFS spectra were acquired at the Canadian Light Source, which is supported by the Canada Foundation for Innovation, Natural Sciences and Engineering Research Council of Canada, the University of Saskatchewan, the Government of Saskatchewan, Western Economic Diversification Canada, the National Research Council Canada, and the Canadian Institutes of Health Research. We acknowledge use of the routine operation data from the Atmospheric Radiation Measurement Climate Research Facility at the Southern Great Plains site of OBER (http://www.archive.arm.gov). We acknowledge use of the NOAA Air Resources Laboratory for the provision of the HYSPLIT transport and dispersion model and READY website (http://www.ready.noaa.gov) used in this publication.

## Author contributions

B.W., D.S.P., M.K.G. and A.L. designed the study. B.W., T.H.H., S.T.K. and M.K.G. performed the experiments and analysis. M.K. provided input and NEXAFS data on soil samples. S.C. and L.K. performed the TEM experiments. B.W.A. performed helium ion microscopy imaging. B.W., S.C., M.K.G. and A.L. wrote the manuscript with contributions from all co-authors.

## Additional information

Supplementary information is available in the online version of the paper. Reprints and permissions information is available online at www.nature.com/reprints. Correspondence and requests for materials should be addressed to A.L.

## Competing financial interests

The authors declare no competing financial interests.

## Methods

**Sample collection.** Samples were collected at Southern Great Plains site in Lamont, Oklahoma, USA. This site was established by the Atmospheric Radiation Monitoring Program of the US Department of Energy. A four-stage Sioutas Cascade Impactor (SKC) was used for sampling. Each stage was preloaded with silicon nitride membrane substrates ($Si_3N_4$ membrane windows, Silson) and carbon-filmed substrates (Copper 400 mesh grids coated with Carbon Type-B films, Ted Pella). Particles collected on substrates placed on the D stage (cutoff 0.25 μm) were analysed. Samples were collected through a sampling inlet located at a height of 10 m, with a 9 l $min^{-1}$ sampling rate for 20 min starting at 19:00 GMT on the dates listed in Supplementary Table 1.

**Chemical imaging of particles.** An environmental scanning electron microscope (ESEM, Quanta 3D model, FEI) with an EDAX energy dispersive X-ray (EDX) spectrometer and a Si(Li) detector with a 10 $mm^2$ active area and an ATW2 window was used[31–33]. Under vacuum conditions, particles were imaged using secondary electron (SE) and forward scattered transmitted electron (STE) signals. The STE signal was also used for imaging when the instrument was operated in the environmental mode, where a controlled amount of water vapour was present as a background gas. The SE imaging mode is inherently sensitive to the surface topography of a specimen and, therefore, was used to provide better imaging contrast for particle surface features. The STE imaging mode is sensitive to the vertical dimensions of particles and was used to distinguish between solid (spherical) and liquid (flattened) particles. In addition to the standard position of the sample normal to the direction of the electron beam (0° tilt of the sample), particles were also imaged at a tilt angle of 75°, allowing visualization of their vertical dimension. A helium ion microscope (Orion NanoFab, Zeiss) was used for surface imaging with enhanced material contrast of the thin organic coating on some of the ASOP. For computer-controlled (CC) SEM/EDX analysis, particles on the substrates were identified and imaged using the STE imaging mode. Then, an X-ray spectrum for each identified particle was acquired at an acceleration voltage of 20 kV and at a beam current of 430 pA for 10 s. Area equivalent diameters (AED) were calculated from the 2D projection area recorded for each individual particle. Particle elemental composition was quantified and is reported in units of atomic fractions. More details on CCSEM/EDX analysis and X-ray mapping of particles are reported elsewhere[11,12,31,34,35]. An FEI Titan environmental transmission electron microscope (TEM, FEI) operated at 300 kV was used to perform high-resolution TEM imaging.

Scanning transmission X-ray microscopy (STXM) uses a focused soft X-ray beam generated from the synchrotron light source to probe chemical bonding of specific elements of interest within individual particles. A set (stack) of STXM images is obtained by raster scanning the sample at fixed photon energy and recording the intensities of the transmitted X-rays at each pixel. The spatially resolved near-edge X-ray absorption fine struture (NEXAFS) spectra are then retrieved for the specific areas of interest from the recorded STXM stacks. Mixing state and chemical bonding of elements within individual particles at ~35 nm size resolution can be identified by analysing the recorded spectra. Carbon, oxygen and nitrogen K-edge NEXAFS spectra were acquired in this study. Further details on the applications of this technique to atmospheric particles and additional information on the STXM instrument are published elsewhere[36–38].

**X-ray spectroscopy of soil samples.** Soils for C NEXAFS analysis were collected at the Hyslop Field Laboratory (Oregon State University). The soil (fine silty mixed superactive mesic Aquic Argixeroll) is moderately drained, medium-textured, and at present under cultivation with Triticum spp. A-horizon material (depth = 10–30 cm) was collected, sieved (2 mm), air-dried, and stored until further use.

To isolate the 'free light' fraction, a density separation procedure was employed that relies on a density gradient established in sodium polytungstate solution. This solution was used to separate mineral-associated organic carbon (heavy fraction) from lower-density organic matter (free light fraction)[39,40]. A density cutoff of $<1.65$ g $cm^{-3}$ was chosen to ensure the exclusion of low-density (~1.7 g $cm^{-3}$) metal–organic complexes and co-precipitates, and the free light fraction samples were freeze-dried for subsequent C NEXAFS analysis.

For C NEXAFS analysis of the free light fraction, subsamples were suspended in MilliQ $H_2O$, deposited onto pre-cleaned indium foils, and air-dried at room temperature. C NEXAFS spectra were collected using the spherical grating monochromator (SGM) beamline 11ID-1 at the Canadian Light Source (CLS)[41,42]. To minimize X-ray exposure, spectra were collected in step scan mode (in 0.25 eV steps from 270 to 320 eV) with a dwell time of 20 ms. After each scan, the beam was moved to a new spot on the sample, collecting a total of 50–70 scans for each sample. The beamline exit slit was set at 25 mm and fluorescence yield data were collected using a two-stage microchannel plate detector. After averaging the scans for each sample, the pre-edge region (270–275 eV) of the average spectrum was set to zero (baseline normalization) and the resulting spectrum ($I$) was normalized to the beamline photon flux ($I_o$) recorded for a separate Au reference foil. The spectrum was referenced to the carboxylic acid peak (288.5 eV) of a citric acid standard for energy calibration.

## References


31. Laskin, A., Cowin, J. P. & Iedema, M. J. Analysis of individual environmental particles using modern methods of electron microscopy and X-ray microanalysis. *J. Electron Spectrosc. Relat. Phenom.* **150,** 260–274 (2006).
32. Laskin, A. *et al*. Tropospheric chemistry of internally mixed sea salt and organic particles: surprising reactivity of NaCl with weak organic acids. *J. Geophys. Res. Atmos.* **117,** D15302 (2012).
33. Wang, B. *et al*. Reactivity of liquid and semisolid secondary organic carbon with chloride and nitrate in atmospheric aerosols. *J. Phys. Chem. A* **119,** 4498–4508 (2015).
34. Knopf, D. A. *et al*. Microspectroscopic imaging and characterization of individually identified ice nucleating particles from a case field study. *J. Geophys. Res. Atmos.* **119,** 10365–10381 (2014).
35. Laskin, A. in *Fundamentals and Applications in Aerosol Spectroscopy* (eds Signorell, R. & Reid, J.) 463–491 (Taylor and Francis Books, 2010).
36. Hopkins, R. J., Tivanski, A. V., Marten, B. D. & Gilles, M. K. Chemical bonding and structure of black carbon reference materials and individual carbonaceous atmospheric aerosols. *J. Aerosol Sci.* **38,** 573–591 (2007).
37. Moffet, R. C. *et al*. Microscopic characterization of carbonaceous aerosol particle aging in the outflow from Mexico City. *Atmos. Chem. Phys.* **10,** 961–976 (2010).
38. Moffet, R. C., Tivanski, A. V. & Gilles, M. K. in *Fundamentals and Applications in Aerosol Spectroscopy* (eds Signorell, R. & Reid, J. P.) 419–462 (Taylor and Francis Books, 2010).
39. Moni, C., Derrien, D., Hatton, P. J., Zeller, B. & Kleber, M. Density fractions versus size separates: does physical fractionation isolate functional soil compartments? *Biogeosciences* **9,** 5181–5197 (2012).
40. Swanston, C. W. *et al*. Initial characterization of processes of soil carbon stabilization using forest stand-level radiocarbon enrichment. *Geoderma* **128,** 52–62 (2005).
41. Regier, T. *et al*. Performance and capabilities of the Canadian Dragon: the SGM beamline at the Canadian Light Source. *Nucl. Instrum. Methods Phys A* **582,** 93–95 (2007).
42. Regier, T. *et al*. in *AIP Conf. Proceedings Synchrotron Radiation Instrumentation* Vol. 879 (eds Choi, J. Y. & Rah, S.) 473–476 (AIP Publishing, 2007).